

Multicopy Crystallographic Refinement of a Relaxed Glutamine Synthetase from *Mycobacterium tuberculosis* Highlights Flexible Loops in the Enzymatic Mechanism and Its Regulation[†]

Harindarpal S. Gill, Gaston M. U. Pfluegl, and David Eisenberg*

Howard Hughes Medical Institute, UCLA-Department of Energy Laboratory of Structural Biology and Molecular Medicine, Departments of Chemistry and Biochemistry and Biological Chemistry, Box 951570, University of California, Los Angeles, California 90095-1570

Received March 29, 2002; Revised Manuscript Received May 28, 2002

ABSTRACT: The crystal structure of glutamine synthetase (GS) from *Mycobacterium tuberculosis* determined at 2.4 Å resolution reveals citrate and AMP bound in the active site. The structure was refined with strict 24-fold noncrystallographic symmetry (NCS) constraints and has an *R*-factor of 22.7% and an *R*-free of 25.5%. Multicopy refinement using 10 atomic models and strict 24-fold NCS constraints further reduced the *R*-factor to 20.4% and the *R*-free to 23.2%. The multicopy model demonstrates the range of atomic displacements of catalytic and regulatory loops in glutamine synthesis, simulating loop motions. A comparison with loop positions in substrate complexes of GS from *Salmonella typhimurium* shows that the Asp50 and Glu327 loops close over the active site during catalysis. These loop closures are preceded by a conformational change of the Glu209 β-strand upon metal ion or ATP binding that converts the enzyme from a relaxed to a taut state. We propose a model of the GS regulatory mechanism based on the loop motions in which adenylation of the Tyr397 loop reverses the effect of metal ion binding, and regulates intermediate formation by preventing closure of the Glu327 loop.

The product of the *glnA1* gene from *Mycobacterium tuberculosis*, glutamine synthetase (GS),¹ is observed extracellularly during the early stages of infection (1, 2). TB-GS is thought to be necessary for the synthesis of poly(L-glutamine-L-glutamate) chains (1), a constituent unique to pathogenic mycobacterial cell walls. These chains comprise 10% of bacterial mass and are tightly associated with the peptidoglycan layer of the cell wall (3). Two similar bacterial GS inhibitors, L-methionine-*S*-sulfoximine and phosphinothricin, have been shown to selectively inhibit extracellular TB-GS molecules and thereby disrupt normal cell wall development (4), suggesting that TB-GS is an attractive target for drug therapy.

In its active state, bacterial GS catalyzes the ATP-dependent condensation reaction of ammonium and glutamate to form glutamine, ADP, phosphate, and a hydrogen ion (a process termed the “biosynthetic reaction”). To be in this

active state, GS requires two enzyme-bound divalent cations, either magnesium or manganese ions, which play both structural and catalytic roles (5). These metal ion binding sites are termed the n1 and n2 sites. The reaction proceeds as an ordered, sequential two-step mechanism (6–10). In the first step, a tightly bound, activated intermediate γ-glutamyl phosphate (Glu~P) is formed as the terminal phosphate of ATP is transferred to the carboxylate side chain of the substrate glutamate (9). In the second step, an enzyme-bound ammonium ion is deprotonated, forming ammonia that attacks the carbonyl carbon of Glu~P to form a tetrahedral intermediate at the transition state. The enzyme subsequently releases free phosphate to yield glutamine (9).

The structure of GS from a mutant *Salmonella typhimurium* strain, unable to adenylylate GS (11), was initially determined to 3.5 Å resolution by X-ray crystallography (12). The structure has been subsequently refined and the resolution extended to 2.5 Å (13, 14). *Salmonella* GS has a molecular mass of 620 kDa and is a dodecamer with 622 symmetry (12, 15), formed from two hexameric rings stacked face to face. Each of the 12 active sites is formed between two adjacent subunits within a ring and is described as a “bifunnel.” ATP enters the bifunnel from the exposed outer surface of the dodecamer, near the 6-fold axis of symmetry. Glutamate enters the opposite end of the bifunnel, at the interface of the hexameric rings, near the 2-fold axes. The n1 and n2 binding sites are located at the joint of the bifunnel.

Ginsburg and Stadtman (5, 16) in the early 1970s identified a “relaxed”, or metal ion-free, GS. This is in an inactive state of the enzyme characterized by its ability to bind AMP

[†] This work was supported by the National Institutes of Health (Grant GM-31299) and the Department of Energy (Grant DE-FC03-87ER60615). We thank the NIH and HHMI for support.

* To whom correspondence should be addressed. Phone: (310) 825-3754. Fax: (310) 206-3914. E-mail: david@mbi.ucla.edu.

¹ Abbreviations: AMP, adenosine monophosphate; ATP, adenosine triphosphate; CA, α-carbon; flap, residues 324–329 (residue numbering of *S. typhimurium* and *E. coli* glutamine synthetase); Glu~P, γ-glutamyl phosphate or the intermediate of the biosynthetic reaction; GS, glutamine synthetase; GS₀, fully unadenylylated glutamine synthetase; GS₁₂, fully adenylylated glutamine synthetase; latch, residues 50–64 (residue numbering of *S. typhimurium* and *E. coli* glutamine synthetase); NCS, noncrystallographic symmetry; PPT, phosphinothricin; PPT~P, phosphinothricin phosphate; rmsd, root-mean-square deviation; TB-GS, glutamine synthetase from *M. tuberculosis*.

but not ATP (5). The binding of AMP was attributed strictly to hydrophobic forces, the phosphate group of AMP not participating. They found metal ions induce structural changes in the active site, resulting in a highly stable and active "taut" form (5). The taut form can be converted back to the relaxed form by incubation with 0.01 M EDTA. The addition of metal ions to the relaxed state induces GS molecules to stack into long tubular rods, as seen in electron micrographs of *Escherichia coli* GS (15); stacking is inhibited by the presence of 0.1 M KCl. Because unadenylylated GS prefers magnesium over manganese for optimal activity and adenylylated GS requires manganese, the role of metal ion binding to GS may be regulatory (5). Other distinguishing properties of the relaxed form include a sedimentation coefficient 0.6 S slower than that of the taut form, an increased level of tryptophan exposure to solvent, and susceptibility to dissociation into monomers upon treatment with 1.0 M urea or alkaline treatment (5).

Adenylation of residue Tyr397 alters several catalytic and physical properties of GS. (1) The rate-limiting step in the biosynthetic reaction changes from product release catalyzed by fully unadenylylated GS₀ to intermediate formation catalyzed by fully adenylylated GS₁₂ (17). (2) The pH optimum for the reaction is lowered from 7.5 to 6.5 (5). (3) The metal ion specificity switches from magnesium to manganese as mentioned above (5), and (4) the apparent affinity of the n1 site for manganese decreases by ~1 order of magnitude, which can also be caused by pH-induced structural changes in the enzyme (5). Regardless, the characteristics of binding and inhibition of GS by the glutamate analogue phosphinothricin are not influenced by adenylation (14, 18).

Here we offer insight into the unusual mechanism by which relaxation and adenylation regulate bacterial GS and extend our model (14) of how phosphinothricin inhibits bacterial GS now in an adenylylated state. Our goal is to provide a basis for future work in computational drug design for the development of TB-specific drugs. In addition, we take advantage of the 24-subunit copies of TB-GS in the crystal asymmetric unit to show how multicopy refinement can be used to elucidate the mechanism. The multicopy refinement is controlled by a novel script that generates a multicopy model refined with strict NCS constraints. This approach may be useful for determining structures with flexible domains or a high copy number in the asymmetric unit.

EXPERIMENTAL PROCEDURES

TB-GS Expression and Activity Assay. The *glnA1* gene from *M. tuberculosis* was subcloned into a traditional *E. coli* expression vector, pTrcHisB (Invitrogen). *E. coli* strain YMC21E, a glutamine auxotroph, was used to express recombinant (r) TB-GS. This strain also lacks adenylyltransferase activity due to the insertion of transposon Tn5 into the *glnE* gene (19). Cells were grown in a 150 L New Brunswick IF250 fermentor (Molecular Biology Institute Fermentor Facility), induced with 0.1 mM IPTG, and then visually checked for expression of a 58 kDa product by SDS-PAGE. Proper folding and functionality of rTB-GS were confirmed in vivo by demonstrating that rTB-GS could restore growth of the auxotroph on minimal media; i.e., the

product of the *M. tuberculosis* *glnA* gene complements the *E. coli* Δ *glnA*(A-G) mutation, and in vitro by both the biosynthetic and transferase assays.

Molecular Replacement Solution. As reported in a preliminary communication (20), data were collected on rTB-GS crystals in space group $P2_12_12_1$ with unit cell dimensions of 207.7 Å × 257.7 Å × 274.5 Å. A Matthews coefficient (21) of 2.89 Å³/Da was calculated on the basis of two TB-GS molecules with a combined molecular mass of 1.3 MDa in the asymmetric unit. The self-rotation function indicated 622 symmetry, found for other bacterial GS dodecamers. The two dodecamers of the asymmetric unit have both 2-fold axes and 6-fold axes parallel to each other. Furthermore, the 6-fold axes appeared to be aligned with the crystallographic *a*-axis. A native Patterson map revealed only one large peak, indicating that the dodecamers in the asymmetric unit are indeed related by a simple translation.

The structure of TB-GS was determined using molecular replacement (XPLOR version 3.843). To find the orientation of the two dodecamers, cross-rotation searches were performed using a model of *S. typhimurium* GS (14) as a probe with nonconserved residues truncated to alanine, as justified by the sequence similarity. The tentative orientation was refined with the Patterson correlation (PC) refinement algorithm (XPLOR version 3.843). To determine the position of one of the two dodecamers in the asymmetric unit, the highest-scoring orientation of the PC refinement was applied to the *S. typhimurium* dodecamer that was subjected to a translation search. To determine the position of the second dodecamer, we used a dodecamer in the same orientation as the first as justified by the $\kappa = 180$ section of self-rotation calculations and the observation that there is only one large peak in a native Patterson map (20). The position of the first dodecamer was fixed, and a partial translation function gave the position of the second dodecamer. The hexamer axes were actually found to be tilted 7.6° away from the crystallographic *a*-axis, and the distance between the positioned dodecamers (119 Å) agrees with the result of the native Patterson calculation. The *R*-factor for the starting model was 55% for reflections in the resolution range of 15–4 Å.

Phase Improvement, Maps, and Model Building. Rigid body refinement with XPLOR version 3.843 brought the initial *R*-factor down to 49%. The molecular replacement probe was then truncated to one subunit. A cross-validation test set was chosen by picking reflections equally distributed over the resolution range. In addition, for each chosen reflection, all neighboring reflections within a box and their NCS-related reflections were excluded from the working set and included in the test set.² The test set consists of 10% of the total reflections. Initial positional and *B*-factor refinement, with 24-fold NCS constraints imposed on the subunit, yielded an *R*-factor of 38% and an *R*-free of 40%. Model building was then implemented, using the program ONO (22). The model was built into 24-fold NCS-averaged maps, with an example portion shown in Figure 1. Maps were calculated by the sigmaA-weighted protocols in XPLOR version 3.843,

² The difference between *R*-factor and *R*-free, when excluding neighboring reflections and NCS-related reflections in the test set, drops to approximately 1% according to our earlier models of *S. typhimurium* GS (unpublished).

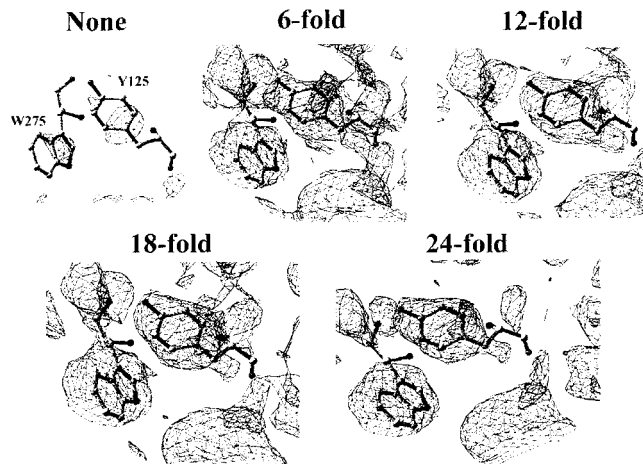


FIGURE 1: TB-GS map averaging. The power of the 24-fold noncrystallographic symmetry (NCS) averaging on the TB-GS electron density is illustrated for the region of Y125 and W275. $F_o - F_c$ electron density maps are shown, where F_o represents the observed structure factors from the TB-GS data set and F_c represents the calculated structure factors of a truncated alanine *S. typhimurium* GS model. Residues Y125 and W275 of TB-GS have been inserted into the density. The electron density for F225 (without the inserted model) can also be seen at the lower right. These residues are not conserved between species. The R -factor at this point was 38%. Notice the dramatic improvement in the maps between no averaging at all and averaging over only six subunits. As the number of subunits used in calculating the averaged maps increases, the clarity of the map improves.

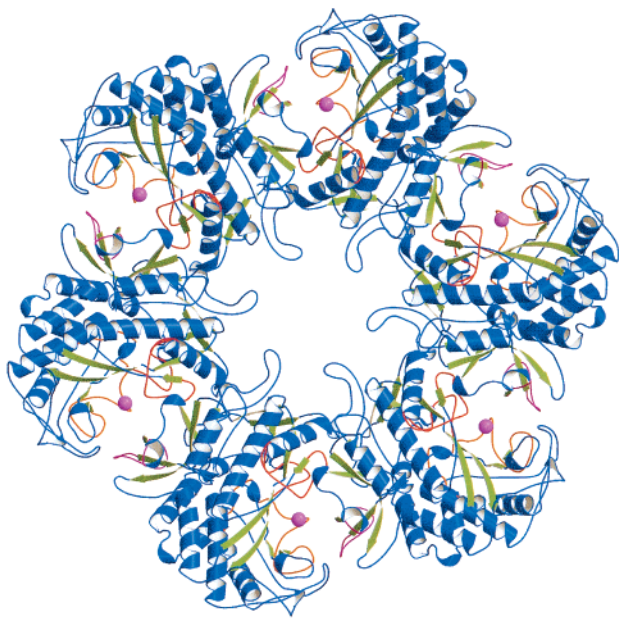


FIGURE 2: TB-GS model. Shown is one of the two hexamer faces of the dodecamer. The flexible catalytic loops are color-coded: the Asp50' latch (residues 50–64, on the adjacent subunit) in each active site is the red loop closer to the solvent channel; the Glu327 flap (residues 324–329) is the orange loop behind the manganese ion, and the Asn264 loop (residues 255–267) is the pink loop opposite the flap. Helices and other loops are blue; β -sheets are green, and the manganese ion at the n2 site is magenta. The model was generated with the program MOLSCRIPT (26).

with a resolution range of 20–2.4 Å. Map averaging was calculated by the program suite RAVE (23). Because of program limitations, each hexamer of the dodecamers was separately averaged using a mask made from one subunit,

Table 1: Data Collection and Atomic Refinement Statistics for TB-GS^a

data	
resolution (Å)	20–2.4
no. of unique reflections	566370
redundancy	4.6
completeness (%)	99.6
model	
no. of atoms per subunit	4078
no. of residues and small molecules per subunit (non-hydrogen)	
protein	477
water	263
manganese ion	1
citrate molecule	1
AMP molecule	1
refinement parameters	
single-subunit model	
R -factor ^b (%)	22.7
R -free (%)	25.5
B_{average} (Å ²)	33.1
deviation from ideality (rmsd)	
bonds (Å)	0.006
angles (deg)	1.4
dihedrals (deg)	25.0
impropers (deg)	1.16
data to parameter ratio ^c	35:1
10-copy model	
R -factor ^b (%)	21.4
R -free (%)	24.5
10-copy model after optional B -factor refinement	
R -factor ^b (%)	20.4
R -free (%)	23.2
B_{average} (Å ²)	24.3
deviation from ideality (rmsd) ^d	
bonds (Å)	0.009
angles (deg)	1.5
data to parameter ratio ^c	3.5:1

^a A single subunit of TB-GS was refined with strict 24-fold NCS constraints imposed on it. To capture the multiple conformations of catalytic loops in their relaxed state, we simultaneously refined 10 copies of the entire single-subunit model against the data with strict 24-fold NCS constraints imposed on each copy. In this way, the data to parameter ratio is reduced by a factor of only 10, as opposed to having 24 copies and refining with restraints applied. Both the R -factor and R -free drop by 2.3%. ^b $R = 100(\sum|F_o - F_c|)/(\sum F_o)$, where F_o and F_c are the observed and calculated structure factors, respectively. ^c Apparent values. ^d Calculated on the first copy.

yielding four independent 6-fold NCS-averaged maps. These four averaged maps were further averaged, yielding one 24-fold NCS-averaged map.

Refinement and Model Statistics. The subunit of the TB-GS model built from the averaged map was refined through iterative cycles of subsequent positional and B -factor refinement, applying a strict 24-fold NCS constraint and a bulk solvent correction (XPLOR version 3.843). The final model statistics are given in Table 1. At this point, the single-subunit model was further refined by employing a multicopy refinement protocol: a total of 10 copies of the monomeric model was duplicated, and strict 24-fold NCS constraints were imposed on each copy. The entire ensemble was then simultaneously refined against the data with a fixed overall B -factor and 0.1 partial occupancy assigned to each of the 10 models. The van der Waals energy term in XPLOR was switched-on for each copy and its NCS symmetry mate, and switched-off among the 10 copies. At the beginning of the refinement, all 10 models were placed on top of each other using atomic coordinates of the averaged subunit model: each atom then receives a random velocity, and each chain

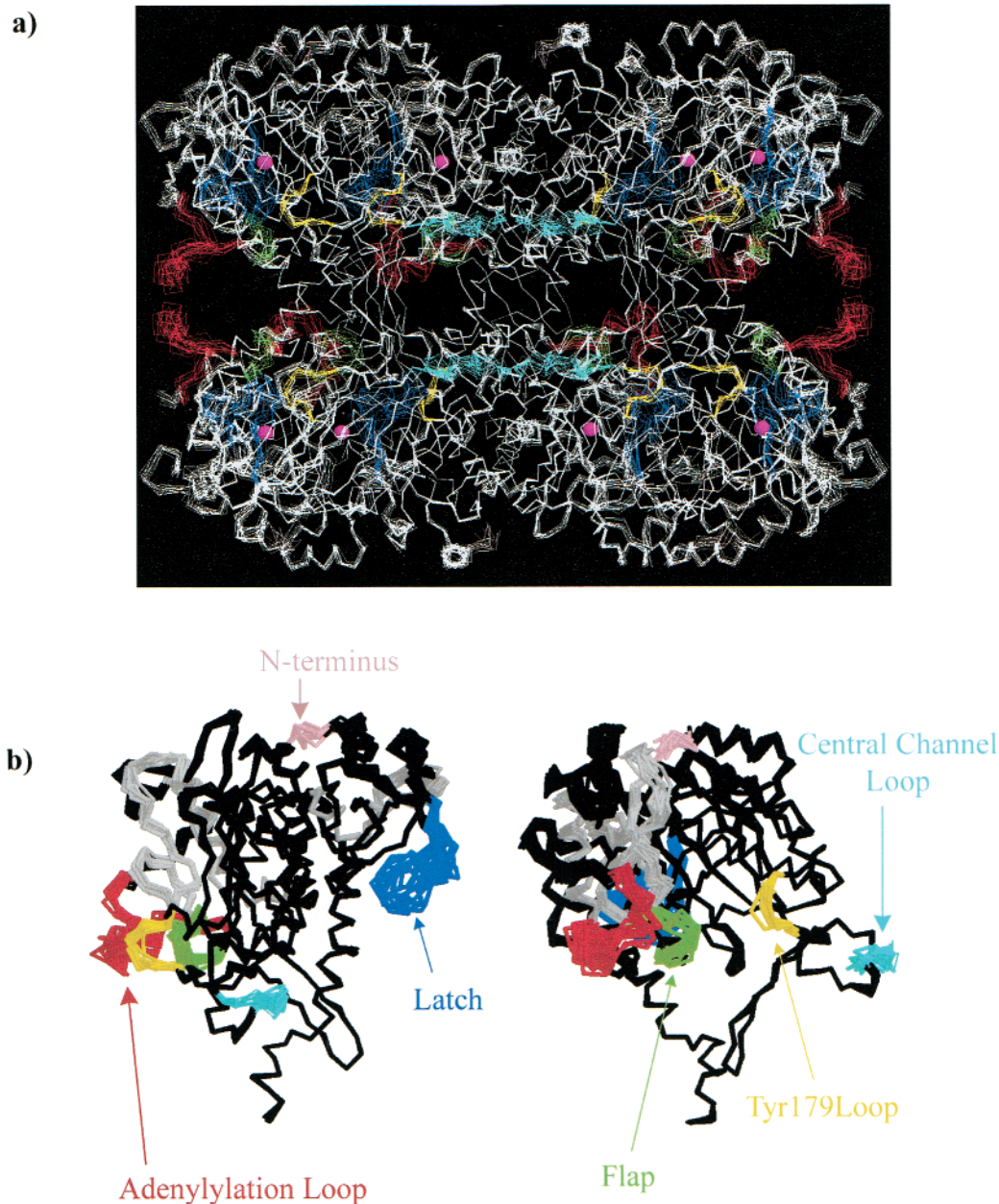


FIGURE 3: Multicopy refined model of TB-GS. The multicopy model illustrates the flexibility and movement of all catalytic and regulatory loops in TB-GS. (a) Ten copies of one GS molecule in the asymmetric unit are superimposed. The model was slabbed so that only the two outer active sites and the two back active sites are visible in each hexameric ring. The coloring of the N-termini and various loops matches the scheme shown in panel b. The manganese ions are shown as pink spheres embedded in each active site. Notice that the varied or disordered regions are not randomly distributed throughout the molecule, but are pronounced in these loops. The adenylation loops (red), for example, can be seen spreading into the solvent between hexamer rings and appearing knob-shaped at their ends. In contrast, the part of the molecule (residues 136–153; the inner β -sheet basket) linking the top and bottom halves of the hexameric rings appears to be well-ordered or like a single chain in the superposition of 10 copies. Approximately 87% of the molecule overlaps with an rmsd of <1.0 . (b) The 10-copy 24-fold NCS-averaged model actually generated by the multicopy refinement is displayed in two orientations. The model to the right is rotated 90° about the vertical axis from the one to the left.

is permitted to diffuse by simulated annealing protocols. The atoms move in a way to minimize the difference in calculated and observed intensities as refined against the data. Positional and *B*-factor refinement were optionally employed to each of the 10 models thereafter. Table 1 also gives the model statistics for the multicopy model. The geometry of both averaged and multicopy models was examined by the program PROCHECK and the PDB validation server. The full asymmetric units were subsequently generated for both models as described by the Protein Data Bank for deposition, as entries 1HTO and 1HTQ, respectively.

RESULTS

Structure Determination. The crystal structure of TB-GS was determined at 2.4 \AA resolution by molecular replacement using the GS model from *S. typhimurium* 1F52 (14) as a probe. The TB-GS model was built and refined using 24-fold NCS averaging, as illustrated in Figure 1. Figure 2 shows a ribbon representation of one hexameric half of the TB-GS dodecamer. A multicopy refinement was then carried out with 10 copies or atomic models, each constrained by strict 24-fold NCS constraints (see Experimental Procedures).

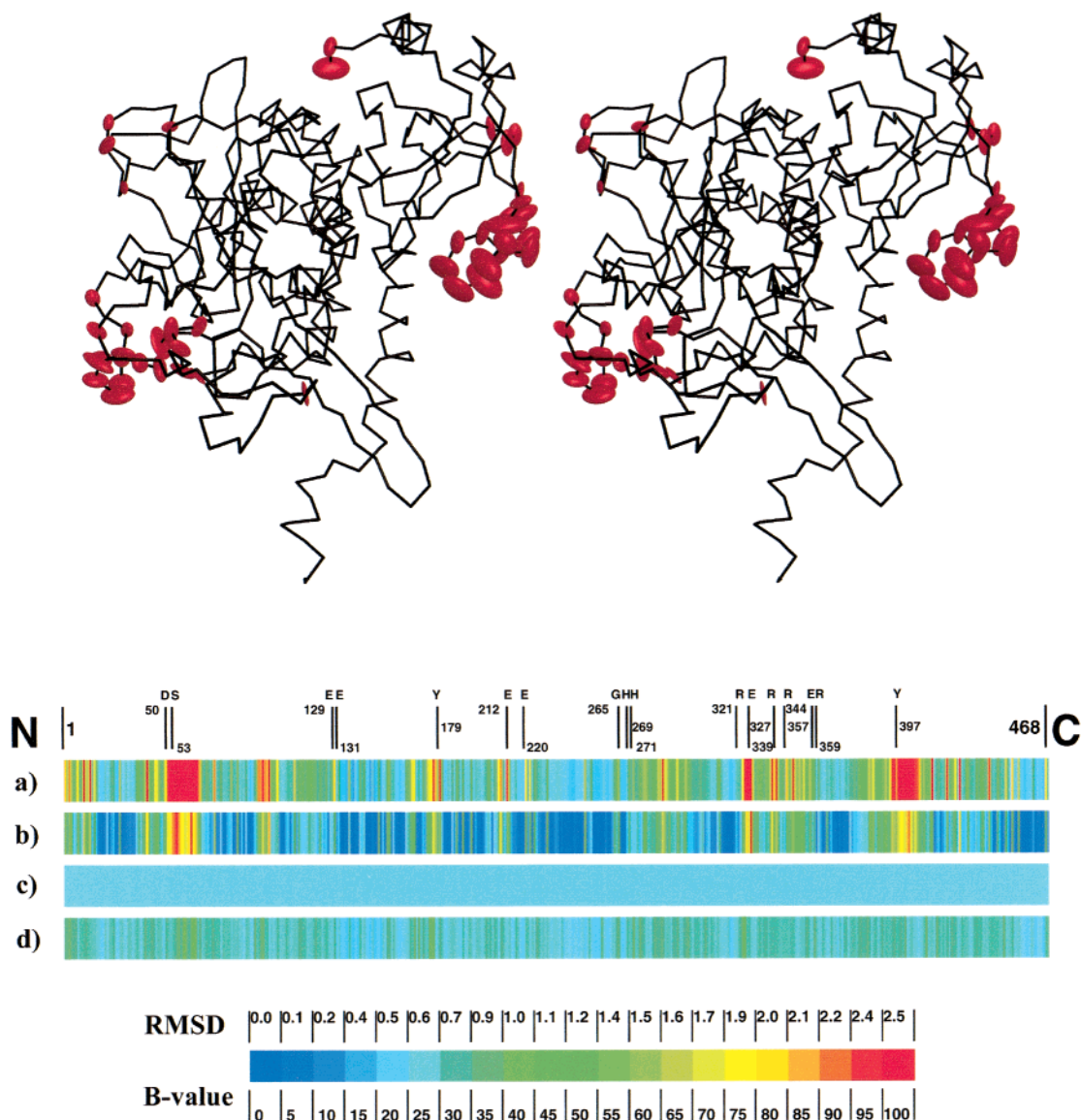


FIGURE 4: Ellipsoid display of the multicopy model. The multicopy model in the same orientation as the left model in Figure 3b is displayed as a stereodiagram and is simplified by an ellipsoid representation of the atomic positions. The shape of the ellipsoids shows the distribution of atoms for the 10 copies and suggests both the latch (right) and the adenylylation loop (lower left) have enough freedom of movement to swing toward each other from neighboring subunits within a ring. The ellipsoids were made by calculating the center of mass for each of the 10 copies per atom and the covariance matrix, which describes the thermal ellipsoid representation of atomic positions. The backbone model is an average of the atomic positions from the 10 copies and is superimposed onto the ellipsoids. The ellipsoids were drawn with the program RASTEP (27). The color chart below compares the rmsd values for each atomic position in the ellipsoid model with the atomic displacement parameters (B -values) for each residue in the single-subunit model. (a) The B -values of the single-subunit model are shown for each CA residue. (b) The rmsd values of the multicopy model are shown for each atomic position. (c) The B -value of the multicopy model is refined to be a constant value (see Table 1) and is depicted as a solid light blue bar. (d) The B -value for each atomic position of the multicopy model is optionally refined after positional refinement (see Experimental Procedures). This bar shows the average B -value among the 10 copies for each atomic position and does not deviate much from the constant value in panel c. Differences between panels c and d may be further minimized by increasing the number of copies used for the multicopy model. Active site residues are indicated by vertical lines above bar a. A color-coded key is shown below that correlates the color of the bars and vertical lines to the rmsd values of the ellipsoid model and B -values of the single-subunit model.

Figure 3 shows the 10 atomic models of the polypeptide backbone superimposed after refinement. Notice that in most regions there is little variation in the 10 backbones. Several loops, however, display significant variation, reflecting the mobilities of these loops. Figure 4 illustrates loop movements by an ellipsoid representation of atomic positions of the multicopy model in stereo. Statistics for the averaged and multicopy models are given in Table 1.

Comparison of TB-GS and *S. typhimurium* GS Models.

(i) *Conformational Differences.* A comparison of the mul-

ticopy TB-GS model with the *S. typhimurium* GS models (14) reveals conformational changes in and structural flexibility of several protein segments surrounding the active site. The major conformational difference between the TB-GS model and the *S. typhimurium* GS models is a shift of the β -strand starting at residue 209 of the β -barrel comprising the lower half of the bifunnel. Because of this shift, residue Glu212 on this strand has moved 10 Å away from the n1 pocket, a ligand of n1 in *S. typhimurium* GS, and now resides outside the active site cavity on the adjoining antiparallel

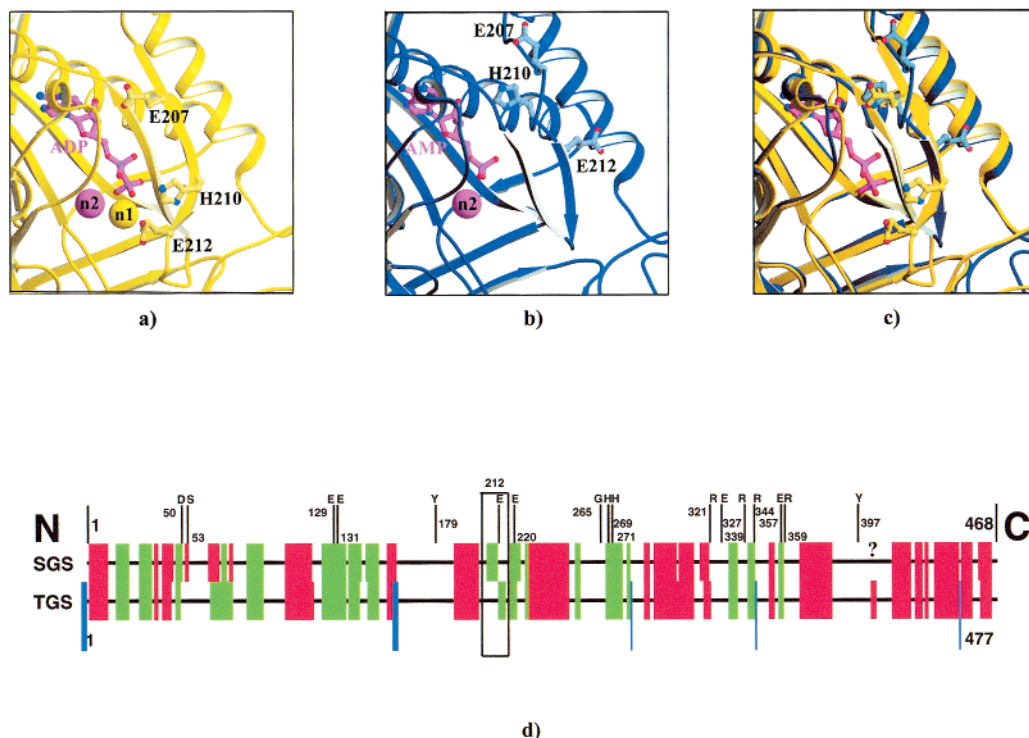


FIGURE 5: Shift of the Glu209 β -strand. The shift of the Glu209 β -strand is shown from its position in the relaxed state to the taut state of GS. (a) The active site of a taut GS, the *S. typhimurium* GS–ADP complex, is shown. The ADP (pink) molecule binds to residues E207 and H210. E212 is also shown as one of the coordinating ligands of the metal ion at the n1 site. (b) The active site of a relaxed GS, the TB-GS model, binds an AMP molecule. Notice the absence of the metal ion at the n1 site and the shift of the Glu209 β -strand, including the new positions of the ligands mentioned in panel a. (c) The models from panels a and b are superimposed to emphasize the shift. The figure was created with the program MOLSCRIPT (26). (d) The secondary structure of TB-GS (TGS) is aligned with that of *S. typhimurium* GS (SGS). The red bars indicate helix regions common to both amino acid sequences, the green bars β -strands, and the black lines loop or coil regions. The thick blue bars indicate two three-residue insertions, and the thin blue bars indicate three single-residue insertions. The shift of the Glu209 β -strand position is boxed. In a taut TB-GS, one would predict the topology around Glu209 to match the *S. typhimurium* GS model, as it does for most of the molecule.

β -strand, the side chain of Glu212 pointing away from the active site altogether (Figure 5). Having lost the metal ligand Glu212, the n1 pockets are empty in TB-GS. Other structural differences between TB-GS and *S. typhimurium* GS coincide with catalytic and regulatory loops whose functions have been described by Eisenberg et al. (19) and Gill et al. (14) and whose flexibilities are demonstrated by the multicopy model in Figures 3 and 4. These include the Glu327 loop (flap, residues 324–329), the Tyr179 loop (residues 153–188 that extend from an active site into the central solvent channel, or toward the 6-fold axis of symmetry), the Asn264 loop (residues 255–267), the Asp50 loop (latch, residues 50–64), and the Tyr397 loop (adenylation loop, residues 388–411).

Electron density in 24-fold NCS-averaged $2F_o - F_c$ maps of the TB-GS model confirms that all five of these loops other than the latch are visible, but in conformations different from those in the *S. typhimurium* GS model. The flap in TB-GS has several discrete conformations as judged by the NCS-averaged maps and reflected by the multicopy model. There is a complete backbone trace of the adenylation loop with an overall atomic displacement temperature factor (80 \AA^2) that is lower than that in the *S. typhimurium* GS model ($\sim 98 \text{ \AA}^2$). Comparison between the models of electron densities for the Asn264 and Tyr179 loops shows that these loops are stabilized next to the latch in the *S. typhimurium* GS model, but peel away from the active site cavity in the TB-GS model where the latch is disordered. The latch in the *S.*

typhimurium GS model appears to be rigid, stabilized next to the active site, as judged by electron density. The average atomic displacement factor for the latch is 75 \AA^2 , highest between residues 50 and 53 where only a backbone trace is visible. On the other hand, the average atomic displacement factor for the latch in the TB-GS model is 96 \AA^2 , built and refined into questionable electron density. Although the multicopy model demonstrates a high degree of disorder for the latch, overall TB-GS has a lower temperature factor and appears to be more ordered than the *S. typhimurium* GS model.

(ii) *Sequence Comparison.* Both *S. typhimurium* GS and TB-GS sequences share similar structural motifs. In terms of amino acid sequence, TB-GS aligns with *S. typhimurium* GS with a level of identity of 52%. All known 19 active site residues are identical. All catalytic loops containing active site residues, such as the flap, the latch, the Tyr179 loop, and the Asn264 loop, have lengths equivalent to those in *S. typhimurium* GS. As shown in Figure 5, the sequence of TB-GS (477 residues/subunit) is longer than that of *S. typhimurium* GS (468 residues/subunit). The N-terminus and the central solvent channel portion of the Tyr179 loop are longer than in *S. typhimurium* GS and account for the most of the additional length. There are no deleted segments in TB-GS compared to *S. typhimurium* GS. The three-dimensional structure of TB-GS superimposes onto *S. typhimurium* GS with an rmsd of 0.94 \AA^2 based upon all CA positions from each structure. Deleting the flap, latch, Tyr179 loop, Asn264 loop, adenylation loop, and the first

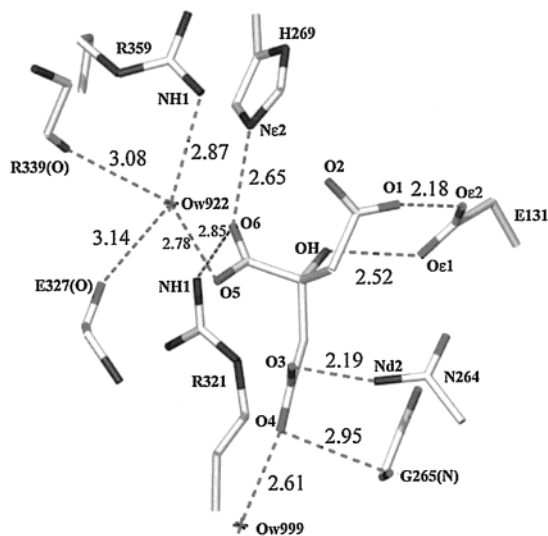


FIGURE 6: Citrate bound in the active site of glutamine synthetase. The binding of a citrate molecule in an active site overlaps with the glutamate-substrate binding site. The oxygens of the citrate molecule (bottom right center) are numbered and labeled. The distances between atoms in the citrate molecule and its ligands are shown in angstroms. Citrate appears to be bound by eight ligands, including two water molecules labeled Ow. The implication for the binding of citrate in the active site is that citrate may be another negative feedback inhibitor of GS, when the enzyme is in an adenylylated or relaxed state, and competes with glutamate for binding during the biosynthetic reaction.

16 overlapping residues of the N-termini in both molecules reduces the rmsd to 0.78 Å².

Other Features. The electron density map shows several small molecules bound to TB-GS. A 24-fold NCS-averaged $2F_o - F_c$ electron density map of the active site reveals a citrate molecule. The citrate is bound by six protein ligands: Glu131(Oe1 and Oe2), Asn264(ND2), Gly265(N), His269(Ne2), and Arg321(NH1). The distances between citrate and its ligands vary from 2.2 to 2.9 Å with an error of 0.32 Å (24) and are illustrated in Figure 6. Either Glu131(Oe1) or citrate(O1) must be protonated to accommodate a hydrogen bond between them. Citrate has a second conformation for binding the same six ligands. Support for this second orientation comes from electron density maps at slightly lower contour levels. The higher-occupancy citrate molecule also appears to bind two waters having low atomic displacement factors. One of the waters (Ow922) is particularly embedded among coordinating ligands Arg359(NH1), Glu327(O), Arg339(O), and citrate(O5), having an atomic displacement factor of 11 Å². Moreover, the 24-fold NCS-averaged difference maps of TB-GS show electron density for adenosine. The density is most likely part of an AMP molecule and is bound in the known nucleotide-binding site located in the top half of the bifunnel. The AMP molecule appears to be bound by hydrophobic forces; no density for the phosphate group is visible. Finally, the helix and loop of *S. typhimurium* GS change to a long β -sheet near the surface of TB-GS (residues 68–80; see Figure 5d).

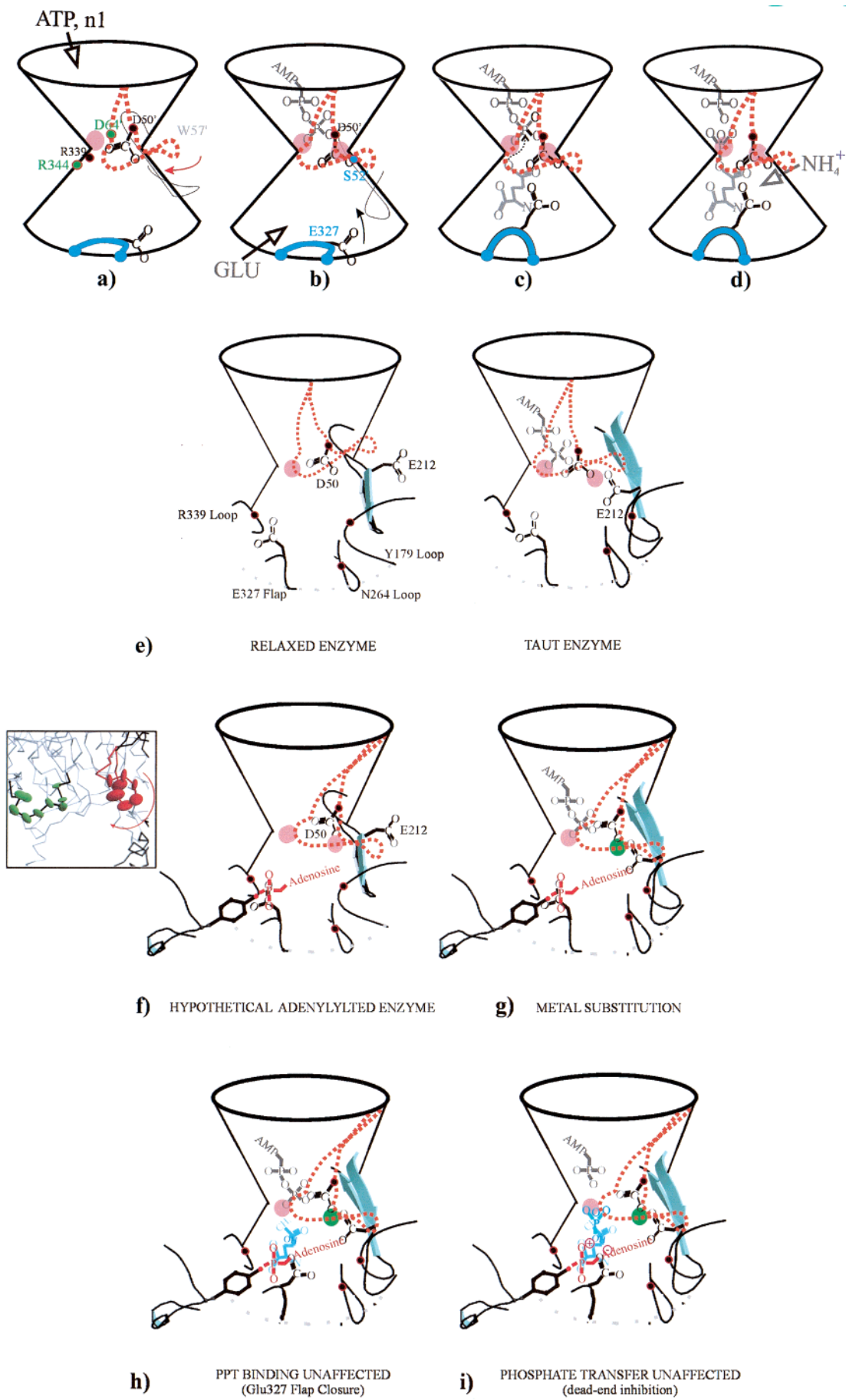
DISCUSSION

TB-GS Is in the Relaxed State. The comparison of the multicopy TB-GS model with the *S. typhimurium* GS models (14) demonstrates the differences in character between the relaxed and taut states of GS described earlier. First, the n1

pockets which in the structure of *S. typhimurium* GS are complexed to manganese are empty in the structure of TB-GS, indicative of the state termed relaxed (5); only half the n2 pockets contain a manganese ion as judged by unaveraged difference maps and by refining the partial occupancy of the manganese ions. Second, comparison of the multicopy TB-GS model with the *S. typhimurium* GS models reveals structural flexibility of several protein segments surrounding the active site, one of which would account for the increased level of tryptophan exposure to solvent observed in the relaxed state of *S. typhimurium* GS from early biochemical work (5). In particular, the increased level of exposure of tryptophan to solvent can be explained by Trp57 in *S. typhimurium* GS on the structural feature we term the latch (residues 50–64). The tip of the latch in TB-GS corresponds to the position of Trp57 in *S. typhimurium* GS and demonstrates the largest degree of movement into solvent by the multicopy TB-GS model. Third, the 24-fold NCS-averaged difference maps of TB-GS showed electron density for adenosine, most likely part of an AMP molecule bound in its nucleotide-binding site located in the top half of the bifunnel, whereas *S. typhimurium* GS has ADP bound here. Consistent with the early observations for a relaxed state of GS (5), the AMP molecule appears to be bound by hydrophobic forces only; so it is reasonable that no density for the phosphate group is visible. An ADP molecule in which only the taut state can bind (10) would require Glu207 and His210 to bind the β -phosphate of ADP as observed in the *S. typhimurium* GS-ADP complex. Hence, ADP binding is not feasible in our TB-GS model because the shift of the Glu209 β -strand comprising these ligands would leave the terminal phosphate groups of an ADP molecule unstabilized and unprotected from hydrolysis. Finally, the helix and loop change to a rather long β -sheet on the surface of TB-GS may reflect tubular stacking formation differences observed between the taut and relaxed states of GS, but could also simply reflect a difference between bacterial GS species (5, 15).

Can the Differences between *S. typhimurium* GS and TB-GS Be Due to Species Change Instead of Relaxation?

There are several lines of evidence that lead us to believe that the overall structural differences between *S. typhimurium* GS and TB-GS are due to conformational changes associated with relaxation as opposed to changes associated with species. First, we expect the structures of both species to be highly similar due to the 52% level of amino acid sequence identity between them. In fact, TB-GS does superimpose onto *S. typhimurium* GS with an rmsd of <1.0 Å² based upon CA positions, despite the conformational differences of the catalytic loops. Therefore, the overall shape of the active site cavity and its substrate entrances remain the same. Second, because all 19 active site residues and lengths of catalytic loops described by Eisenberg et al. (19) are also conserved in the sequence alignments, we expect the mechanism of action to be the same as well. Even the method of regulation of TB-GS appears to be identical to that of *S. typhimurium* GS: the adenylation loop in *M. tuberculosis* is conserved along with the associated regulatory enzymes required for its covalent modification. These strong similarities probably contribute to the transcomplementation growth rate of TB-GS in *E. coli* being nearly identical to that of wild-type GS in *E. coli* (data not shown). Third, studies by



Harth et al. (1) indicate that TB-GS does indeed have a magnesium requirement for optimal activity, and incubation with EDTA causes TB-GS to lose activity, the same as other bacterial GS molecules. Because the known coordinating residues that bind metal in bacterial GS are present in TB-GS, the absence of the metal ions in our model of TB-GS may be explained by the presence of citrate bound in the active site originating from the crystallization condition. Citrate is prone to chelating the metal ions, thereby changing the state of the TB enzyme from taut to relaxed just as EDTA is described in the literature as changing the state of the *E. coli* enzyme.

How Might ATP and n1 Binding Trigger Loop Closures over the Active Site? The binding of ATP and the n1 metal ion indirectly facilitate loop closures to yield a taut GS, through the conformational change of the Glu209 β -strand segment (Figure 7). Both ATP and the n1 ion play a cooperative role in stabilizing the Glu209 β -strand next to the Thr32 β -strand on the adjacent subunit (the prime indicates that the residue is on the adjacent subunit within a hexameric ring), allowing for intersubunit hydrogen bonding between Glu209(O) with Thr32'(N) and Glu209(N) with Thr32'(O) (not shown). This brings the N-terminus of the adjacent subunit that contains the latch closer to the active site (Figure 7a), inducing Arg339 to interact with Asp50' on one end of the latch and inducing Arg344 to interact with Asp64' on the other end of the latch as noted in earlier work by Liaw and Eisenberg (10). The entire latch is thereby largely stabilized next to the active site (Figure 7b). The β -barrel forming the walls of the bifunnel is now complete, with the Asn264 loop and the Tyr179 loop both moving 7 Å to surround the active site cavity around the lower side and back gaps of the bifunnel. These loops are shown in Figure 7e and are located between the latch and the Glu209 β -strand. GS is now in the taut state. When the substrate glutamate binds (Figure 7b), Ser52' at the tip of the latch is positioned within hydrogen bonding distance of Glu327 to bind the flap and completely close the active site entrance from solvent. The flap helps to facilitate phosphate transfer (Figure 7c) and to complete the negatively charged ammonium-binding pocket (Figure 7d) (14).

Are the Regulatory Effects of Relaxation and Adenylylation Related? The relaxed state of GS as described in the TB-GS model may be structurally similar to the covalently modified adenylylation state of GS (25), and so may the end effects of relaxation and adenylylation. We can use the multicopy ellipsoid model in Figure 4 to make a picture of the active site in the adenylylated state to compare with the relaxed state (see Figure 7f). Notice that the adenylylation loop and the adjacent latch within the same hexameric ring swing toward one another, as suggested by the elongated shape of the ellipsoids. Interaction between the latch and the AMP moiety was also suggested by Almasy et al. (12) and Reynaldo et al. (30). The ellipsoid model suggests that the adenylylation loop with an AMP moiety attached to Tyr397 (25) interacts with the adenylylation loop within the same hexameric ring as opposed to the adenylylation subunit on the opposite ring. In this adenylylated state, the flap, the Asn264 loop, and the Tyr179 loop will not be able to close over the active site or grab onto the latch.

This state in which the latch and other loops are disabled is similar to the relaxed state. First, in both states, the active site flap is disengaged from closing. The competition between the flap and the covalently modified adenylylation loop for interaction with the latch would make the phosphoryl transfer from ATP to glutamate less energetically favorable (17). The reason is that the flap could not close over and align the substrates to facilitate intermediate formation. This agrees with the finding that the rate-limiting step in glutamine synthesis shifts from product release on unmodified GS₀ to intermediate formation on fully adenylylated GS₁₂ (17). In addition, the intermediate would be susceptible to hydrolysis with the active site open. Second, because Asn264 and Tyr179 loop closures cooperate with the complete formation of the n1 site by stabilizing the β -strand in a conformation that positions Glu212 on the β -strand next to the negatively charged pocket, the shift of these loops away from the active site may permit the β -strand to revert to a relaxed position similar to that in the TB-GS model. The affinity for the n1 site would decrease as noted in earlier work (5), because only two ligands, Glu131 and Glu220, would be left to bind the n1 ion. The change in metal ion specificity from a

FIGURE 7: Mechanism of flap closure during glutamine synthesis and a model of adenylylated GS with PPT bound in the active site. A cartoon of the active site of GS in panels a–d suggests the mechanism of the first step in the biosynthetic reaction. The pink circles at the neck of the bifunnel represent the metal ions, and the red dashed loop represents the Asp50' latch, the cyan loop the Glu327 flap, and the thin line the Glu209 β -strand. The residues that hold the loops closed are shown, with every two color-coded residues binding each other: R339 binds D50', R344 binds D64', and E327 binds S52'. The prime denotes that the residue is on the adjacent subunit. The mechanism is described in the text. The position of Trp57' in *S. typhimurium* GS (gray) is marked, the latch movement reflecting the tryptophan fluorescence enhancement upon ATP binding observed from early studies (28, 29). Panel e shows models for the active site in the relaxed and taut states of GS that are more complete than those depicted in panels a and b. The left bifunnel represents the relaxed state of GS, whereas the right bifunnel represents the taut state, with ATP. The relaxed state model of the bifunnel is based on the TB-GS structure, which lacks the divalent cations that stabilize the taut state as seen in *S. typhimurium* GS complexed to ATP. A total of six major loops hover over the lower half of the bifunnel and are stabilized by metal ion and ATP binding. (f) A hypothetical model explains how GS is regulated by adenylylation of Y397, on the adenylylation loop. The active site is drawn so that the 6-fold axis of GS is vertical. The picture of the multicopy model shows an active site of GS, illustrating that the adenylylation loop (with green ellipsoids) and the tip of the latch (with red ellipsoids) are adjacent to each other. The shape of the ellipsoids suggests that both the latch and the adenylylation loop swing toward the active site and come within bonding distance, with an AMP moiety attached to Y397. The adenylylation loop with the modified side chain of Y397 is shown in the cartoon at the bottom left of each active site (bifunnel). The red dashed loop represents the Asp50' latch, and the solid black loop behind the Y397 represents the Glu327 flap (see panel e). The hydrophobic lip of the latch is shown to bind the AMP moiety covalently attached to Tyr397, thereby preventing its closure and the formation of a taut active site. The figure also shows the Glu209 β -sheet (with E212 labeled) and the Tyr179 loop (just below) in relaxed positions. (g) A substitution of the metal ion (magnesium) at the n1 site with a more electronegative metal ion (manganese shown in green) binds E212 and helps to restabilize the Glu209 β -sheet in the active conformation that binds the Tyr179 loop. (h) PPT can now bind in the active site coordinating with the manganese ion. Despite adenylylation, PPT is also able to close the bottom entrance of the bifunnel by directly interacting with the flap and is now poised for phosphorylation by ATP as presented by Gill and Eisenberg (14). (i) The dead-end inhibition of PPT~P is shown in an adenylylated active site of GS, demonstrating the electrostatic forces binding the flap (–) and the inhibitor (+).

magnesium ion at the n1 site to the more electronegative manganese ion (Figure 7g) might stabilize the Glu209 β -strand in the active conformation and therefore account for the restored activity. In short, the effect of adenylation to prevent catalytic loops from forming substrate-binding sites reverses the effect of ATP and n1 binding, mimicking a relaxed state of the enzyme.

Our model of phosphate transfer from ATP to phosphinothricin (PPT), described in Gill and Eisenberg (14), is also consistent with this suggested structural effect of adenylation. Unlike phosphate transfer to glutamate on fully adenylylated GS (GS₁₂), phosphate transfer to PPT is not rate-limiting despite the close resemblance of PPT and glutamate. The notable difference between PPT and glutamate is that PPT has a hydrogen bond donating group at the ϵ -position that interacts with the flap whereas glutamate is lacking this functional group. When PPT binds on GS₁₂, the inhibitor closes the flap by itself (Figure 7h), regardless of the interaction of the modified adenylation loop with the latch. The flap can then facilitate phosphate transfer to PPT, as illustrated in Figure 7a–d, which is similar to its role in the biosynthetic reaction.

Summary. Multicopy refinement appears to be useful for the case of strict NCS-averaged constrained models of asymmetric units, to simulate flexible loops or domains having multiple discrete conformations. The varied conformations seen in the different copies can be interpreted in terms of enzymatic mechanism. In the case of GS from *M. tuberculosis*, the variation of loop structure and the absence of metal ions are consistent with the relaxed form of glutamine synthetase.

ACKNOWLEDGMENT

We thank Kyle Burkhardt at the Protein Data Bank for processing the multicopy model, Dr. Helen Berman and staff for insightfully annotating the multicopy model as an NMR model, Drs. Robert Grothe and Michael Sawaya for discussion, and Dr. Thomas Sutherland for fermentation growth.

REFERENCES

1. Harth, G., Clemens, D. L., and Horwitz, M. A. (1994) *Proc. Natl. Acad. Sci. U.S.A.* 91, 9342–9346.
2. Tullius, M. V., Harth, G., and Horwitz, M. A. (2001) *Infect. Immun.* 69, 6348–6363.
3. Hirschfield, G. R., McNeil, M., and Brennan, P. J. (1990) *J. Bacteriol.* 172, 1005–1013.
4. Harth, G., and Horwitz, M. (1999) *J. Exp. Med.* 189, 1425–1435.
5. Ginsburg, A. (1972) *Adv. Protein Chem.* 26, 1–79.
6. Krishnaswamy, P., Pamiljans, V., and Meister, A. (1962) *J. Biol. Chem.* 237, 2932–2940.
7. Midelfort, C. F., and Rose, I. A. (1976) *J. Biol. Chem.* 251, 5881–5887.
8. Meek, T. D., and Villafranca, J. J. (1980) *Biochemistry* 19, 5513–5519.
9. Meister, A. (1980) in *Glutamine: Metabolism, Enzymology and Regulation of Glutamine Metabolism*, pp 1–40, Academic Press, New York.
10. Liaw, S. H., and Eisenberg, D. (1994) *Biochemistry* 33, 675–681.
11. Bancroft, S., Rhee, S. G., Neumann, C., and Kustu, S. (1978) *J. Bacteriol.* 134, 1046–1055.
12. Almasy, R. J., Janson, C. A., Hamlin, R., Xuong, N., and Eisenberg, D. (1986) *Nature* 323, 304–309.
13. Yamashita, M., Almasy, R., Janson, C., Cascio, D., and Eisenberg, D. (1989) *J. Biol. Chem.* 264, 17681–17690.
14. Gill, H. S., and Eisenberg, D. (2001) *Biochemistry* 40, 1903–1912.
15. Valentine, R. C., Shapiro, B. M., and Stadtman, E. R. (1968) *Biochemistry* 7, 2143–2152.
16. Stadtman, E. R., and Ginsburg, A. (1974) in *The Enzymes* (Boyer, P. D., Ed.) pp 755–807, Academic Press, New York.
17. Abell, L. M., and Villafranca, J. J. (1991) *Biochemistry* 30, 1413–1418.
18. Abell, L. M., and Villafranca, J. J. (1991) *Biochemistry* 30, 6135–6141.
19. Eisenberg, D., Gill, H. S., Pfluegl, G. M. U., and Rotstein, S. H. (2000) *Biochim. Biophys. Acta* 1477, 122–145.
20. Gill, H., Pfluegl, G. M. U., and Eisenberg, D. (1999) *Acta Crystallogr. D* 55, 865–868.
21. Matthews, B. W. (1968) *J. Mol. Biol.* 33, 491–497.
22. Jones, T. A., and Kjeldgaard, M. (1999) *Methods Enzymol.* 277, 173.
23. Kleywegt, G. J., and Jones, T. A. (1999) *Acta Crystallogr. D* 55, 941–944.
24. Luzzati, V. (1952) *Acta Crystallogr.* 5, 802–810.
25. Stadtman, E. R., Smyrniotis, P. Z., Davis, J. N., and Wittenberger, M. E. (1979) *Anal. Biochem.* 95, 273–285.
26. Kraulis, P. J. (1991) *J. Appl. Crystallogr.* 24, 946–950.
27. Merrit, E. B. (1997) *Methods Enzymol.* 277, 505–524.
28. Ginsburg, A., Yeh, J., Hennig, S., and Denton, M. (1970) *Biochemistry* 9, 633–649.
29. Timmons, R., Rhee, S., Luteran, D., and Chock, P. (1974) *Biochemistry* 13, 4479–4485.
30. Reynaldo, L. P., Villafranca, J. J., and Horrocks, N. D. (1996) *Protein Sci.* 5, 2532–2544.

BI020254S